한국전자현미경학회지 제 26 권 제 2 호 1996
Korean J. Electron Microscopy 26(2), 105~121(1996)

종 설

투과전자현미경을 이용한 최근의 재료분석기술

박 경 수 · 홍 순 구 · 신도다이스케*
삼성종합기술원 분석연구실, *일본 토호쿠대학 소재연구소 형태평가연구실

Recent Transmission Electron Microscopy in Materials Analysis

Gyeong-Su Park, Soon-Ku Hong and Daisuke Shindo*
Analytical Engineering Lab., Samsung Advanced Institute of Technology
*ASMA Lab., Institute for Advanced Materials Processing of Tohoku University, Japan
(Received December 5, 1995)

초 록

투과전자현미경을 이용한 최근의 재료 분석기술에 대해 일본 토호쿠대학의 ASMA (Atomic Scale Morphology Analysis) 연구실에서 얻은 실험결과를 중심으로 설명하였다.

현재 토호쿠대학에서 가동 중에 있는 가속전압 1250 kV의 초고압 투과전자현미경은 분해능이 약 0.1 nm이며, 이 전자현미경으로부터 얻은 고분해능상은 대형컴퓨터를 이용한 시뮬레이션에 의해 해석 할 수 있음을 나타내었다. 또한, 이러한 뛰어난 고분해능 특성을 가진 초고압 투과전자현미경과 최근 재료 분야의 전자현미경 시료 제작기술의 하나로서 크게 주목받고 있는 초박절편법(Ultramicrotomy)을 이용한 헤마타이트 미립자의 내부구조 해석 결과를 나타내었다.

새로운 전자현미경 분석기법을 위한 주변장비의 눈에 띄는 발달중의 하나로서 전자현미경상을 디지탈 형태로 기록하고, 이를 효과적인 화상처리 기법으로 해석할 수 있는 Imaging Plate (IP)를 주목할 수 있다. 본 논문에서는 IP의 응용 예로서 IP를 이용하여 기록한 고분해능 전자현미경상과 전자 회절패턴의 정량해석 결과에 대해 나타내었다. 에너지분산 X-선 검출기를 이용한 새로운 분석기법의 예로서 전자 채널링 효과를 이용한 ALCHEMI법을 Ni-Al-Mn계 화합물에 대한 실험결과와 함께 나타내었다. 또한, 전자에너지 손실 분광 분석법을 이용한 최근 분석 결과로서 여러 구리 화합물의 전자구조 차이에 따른 구리의 L_{23} 가장자리 피이크 변화를 나타내었다. 새로운 전자현미경법인 에너지 필터를 사용하여 $Al_{0.5}In_{0.5}As$의 전자회절 패턴의 백그라운드를 제거한 결과를 에너지 필터를 사용하지 않은 $Al_{0.5}In_{0.5}As$의 전자회절 패턴과 비교하여 나타내었다.

Key words : High-voltage electron microscope, Ultramicrotomy, ALCHEMI, Energy filter

I. INTRODUCTION

Electron microscopes have been widely used in many fields of science and technology. Recent progress of materials analysis by transmission electron microscopy has been made together with various improvements on electron microscopes.

One of the notable improvements of the capability in electron microscopes is the resolution limit. The high-voltage, high-resolution electron microscope (JEM-ARM1250) installed in Tohoku university has proved to reach its theoretical point resolution of about 0.1 nm, and thus the atomic arrangements of most materials projected along crystallographic axes can now be resolved directly. It should be also noted that the gun of field emission-type has been newly developed in place of the electron gun with thermal emission-type. The installation of the field emission gun on electron microscopes enables us to obtain an electron probe smaller than 1 nm in diameter, and then to carry out the compositional analysis at interfaces on the atomic scale owing to a lower energy spread and a higher brightness than the conventional guns (Otten, 1994; Bando, 1994).

The increasing application of electron microscopy has also induced rapid developments in specimen preparation techniques. There are a number of techniques on specimen preparation for transmission electron microscopy (TEM), i.e., electropolishing, ionmilling, ultramicrotomy, chemical polishing, crashing and so on. Among them, the ultramicrotomy whose main application was limited to the organic substances in the past recieves much attention recently as its active application to the TEM study of metal alloys (McMahon and Malis, 1993), semiconductor, polymer and ceramics (Watson *et al.*, 1962; Petres *et al.*, 1969). One of the great advantages of ultramicrotomy is known to be the speed and simplicity of specimen preparation. Attempts to slice hard materials by this technique are not new but mechanical damage during sample preparation has been the major concern. However, the newest microtomes can produce quite thin sections (<40 nm) with small artifacts by careful sectioning process, so that the investigations can be carried out on relatively damage-free areas. In addition to ultramicritomy, focused ion beam etching technique has been newly developed. The technique has been successfully applied to the fabrication of TEM specimens of Si based and III-V based semiconductor materials. If specimens consist of different materials distributed inhomogeneously, it is difficult to obtain uniformly thin specimens by other techniques. However, the thin specimens of these materials can be successfully obtained by the focused ion beam etching technique with strong focused ion beam at the local regions. Thus this focused ion beam etching technique is especially useful to investigate boundaries and interfaces by electron microscopy (Pantel *et al.*, 1994; Saka *et al.*, 1994).

Besides the peripheral instruments for electron microscopy have undergone drastic changes. One of the revolution is the emergence of new recording device, such as the imaging plate system (Mori *et al.*, 1990; Oikawa *et al.*, 1990) and the slow scan CCD camera (Ishizuka, 1993; Fan and Ellisman, 1993). In particular, the imaging plates enable us to record images at high sensitivity, wide dynamic range and good linearity to the electron dose in comparison to ordinary photographic films. By coupling these new recording system with a computer network system, quantitative analyses of high-resolution electron microscope images and electron diffraction patterns can be carried out.

In analytical electron microscopy, a new technique, so called ALCHEMI, can be applied successfully to locating additives in various intermetallic compounds by analyzing the electron channeling effect in the energy dispersive X-ray spectroscopy. In the electron energy loss spectroscopy, not only the compositional information

but also the information on the electronic structure of advanced materials can be obtained in short acquisition time.

In this paper, the authors present the experimental results obtained by utilizing aforementioned new instruments and techniques.

High-Voltage, High-Resolution Electron Microscope

One of the most important parameters on the capability of electron microscopes is the resolution limit. In general, the theoretical resolution limit of electron microscopes d is given with

$$d = 0.65 C_s^{1/4} \lambda^{3/4} \qquad (1)$$

where C_s and λ are a spherical aberration constant of the objective lens and the wave length of the incident electrons, respectively. Thus much effort has been devoted to get small values of C_s and to achieve the high resolution of electron microscopes. The theoretical resolution limit of the high-voltage, HREM (JEM-ARM 1250) installed in Tohoku university is estimated to be 0.103 nm. However, the effective resolution limit is influenced by other imaging parameters, such as the chromatic aberration and the beam divergence of the incident electrons. The effective resolution limit can be estimated by investigating a Fourier diffractogram of HREM images of thin amorphous films (Park and Shindo, 1996). Fig. 1(a) and (b) shows the Fourier diffractogram of a HREM image of a Ge thin film obtained by HVEM in Tohoku university near the Scherzer focus and the intensity profile obtained by averaging the square of Fig. 1(a) along the circumference, respectively. From the intensity profile of Fig. 1(b), the change of slope can be seen at the position indicated by an arrow. The position is coincident with the intensity limit of the Fourier diffractogram as indicated by the dotted line in Fig. 1(a). By measuring the spatial frequency q of the position, the effective resolution limit of the electron microscope is estimated to be 9.35 nm^{-1} in the reciprocal space or 0.107 nm in the real space.

By utilizing the high-resolution limit of an

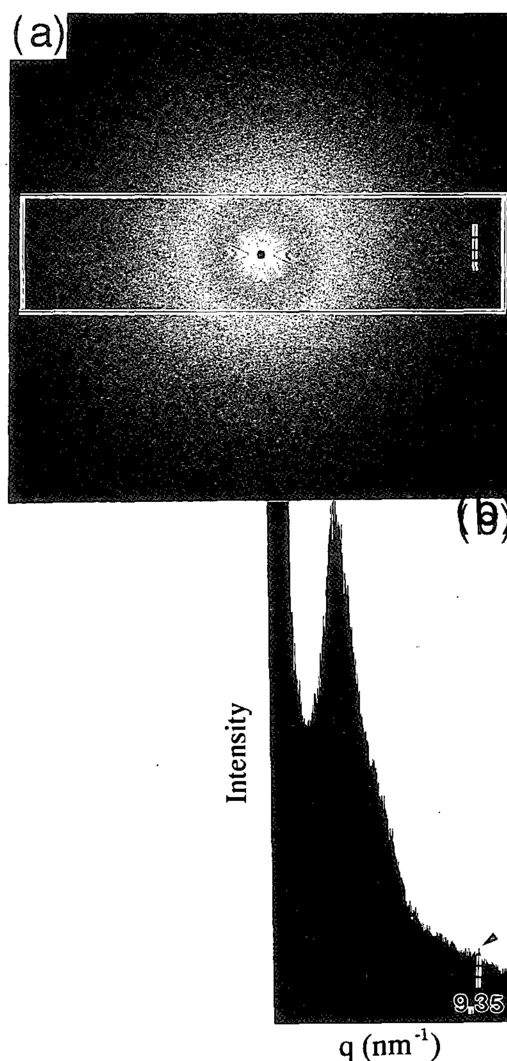

Fig. 1. Fourier diffractogram of (a) HVEM image of a Ge thin film near the Scherzer focus and (b) its intensity profile.

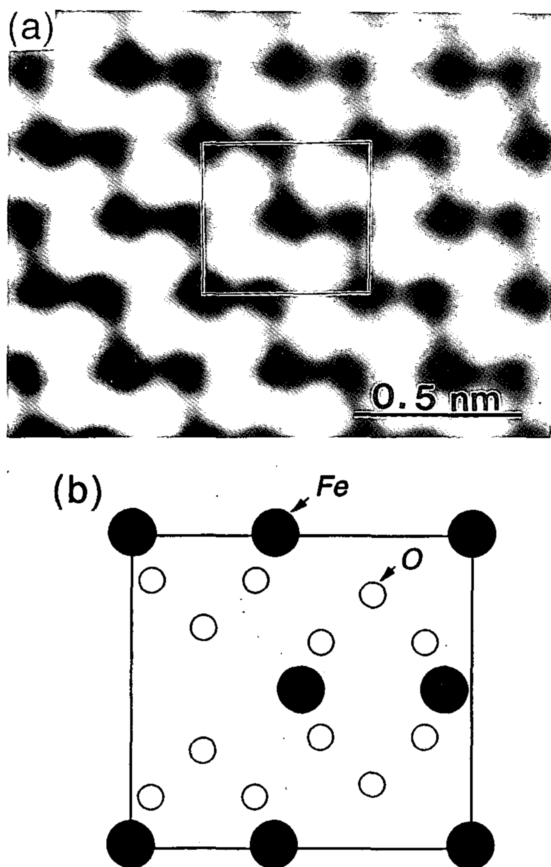

Fig. 2. (a) HREM image of a hematite (α-Fe_2O_3) particle by a high-voltage, HREM with the incident electron beam parallel to the [20$\bar{2}$1] direction.
(b) Model of -Fe_2O_3 structure projected along the [20$\bar{2}$1] direction.

HVEM, the atomic positions of most materials projected along crystallographic axes can now be resolved directly. As one of examples, Fig. 2(a) shows a structure image of a hematite particle obtained by the high-voltage, HREM with the incident electron beam parallel to the [20$\bar{2}$1] direction. In Fig. 2(b), a model of an atomic arrangement of the hematite structure projected along the [20$\bar{2}$1] direction is shown. The arrangement of dark dots in the image of Fig. 2(a) well corresponds to the Fe atom positions of the model in Fig. 2(b) despite of the background contrast of a carbon film. Each square in Fig. 2(a) and (b) indicates a unit cell used for the image simulation. Figure 3 shows simulated images calculated with the parameters listed in Table 1 together with the defocus value of 40~43.5 nm and the crystal thickness of 0.7~8.1 nm. From a comparison between the calculated and real images, it is reasonably concluded that the calculated image by the defocus value of 40~43.5 nm and the crystal thickness of nearly 3.7 nm is well coincident with the observed structure image.

Table 1. Parameters used for computation of images.

Accelerating voltage	1250 kV
Spherical aberration constant	1.6 mm
Chromatic aberration constant	4.1 mm
Objective aperture radius	6 nm^{-1}
Number of beams	32×32

Specimen Preparation Techniques

A number of thinning techniques have been developed for the preparation of TEM samples, for example, ion milling, jet-polishing, crashing and ultramicrotomy. Among them, the authors have recently applied the ultramicrotomy to make thin sections of fine oxide particles (Shindo *et al.*, 1993, 1994; Park *et al.*, 1994, 1995). Under the optimum slicing conditions of ultramicrotomy, successive thin sections of fine oxide particles can be obtained (Park *et al.*, 1994, 1996). As one of examples, Fig. 4(a) shows successive thin sections of the resin containing pseudocubic hematite (α-Fe_2O_3) particles. Enlarged electron microscope images corresponding to the part of each section are shown in Fig. 4(b). It is found from the shapes of these sections that the sections make an angle of about 37 degrees with the surface of the pseudocubic

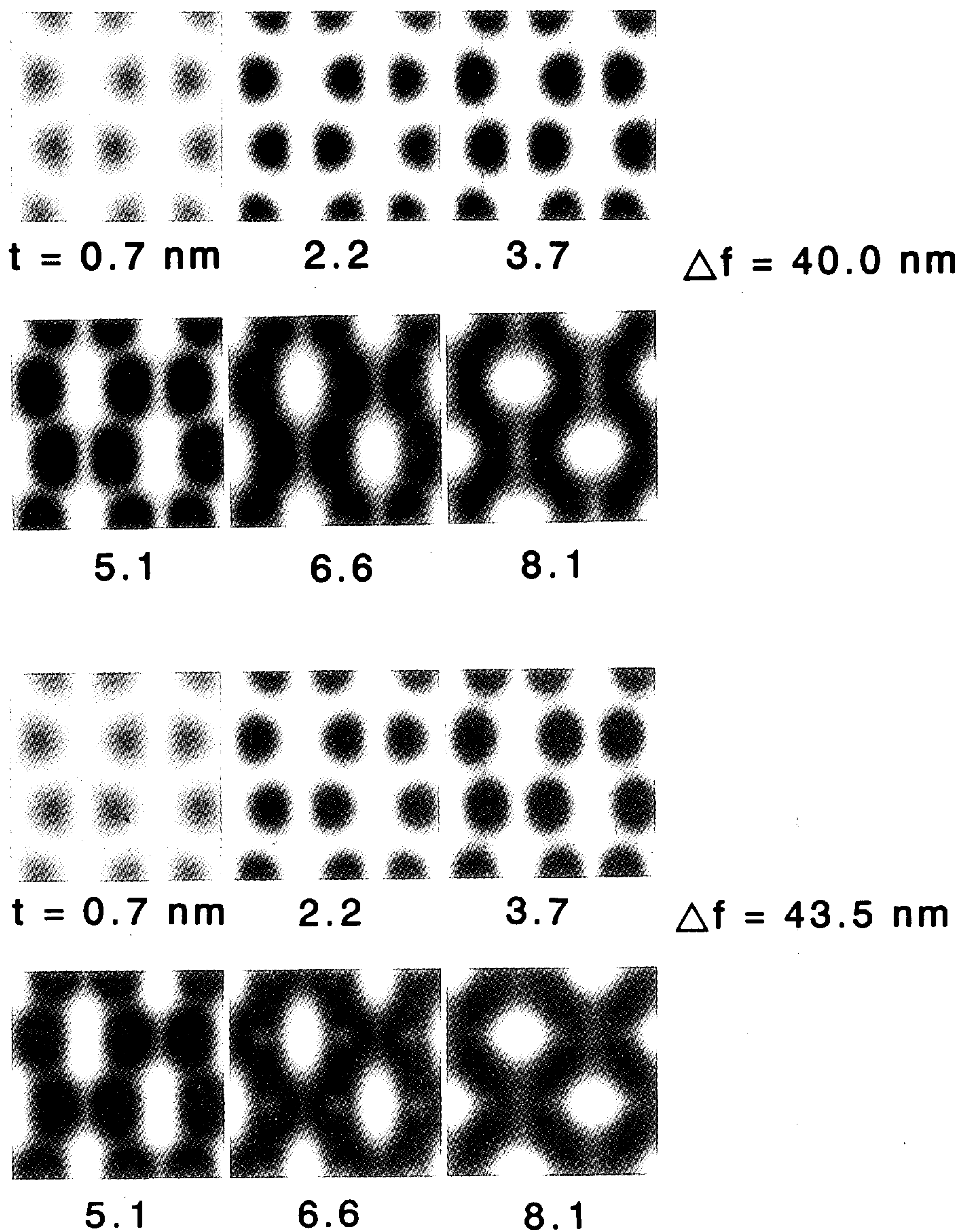

Fig. 3. Simulated images. Δf and t are the defocus value and crystal thickness, respectively.

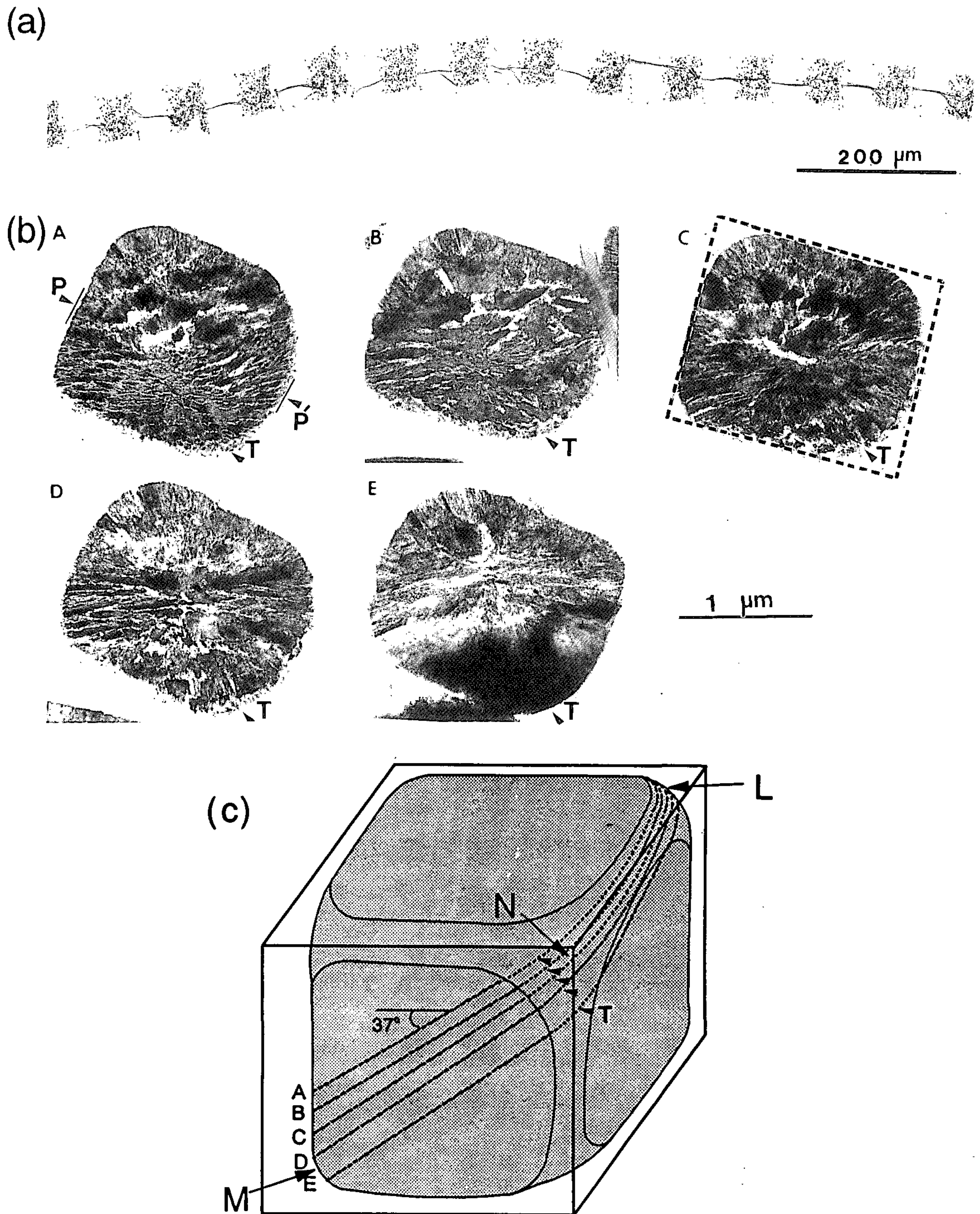

Fig. 4. (a) Transmission electron micrograph of the successive thin sections of the resin containing pseudocubic hematite particles.
(b) Enlarged electron microscope images of the successive thin sections of (a).
(c) Schematic illustration showing the positions of the successive sections of (b) in a pseudocubic particle.

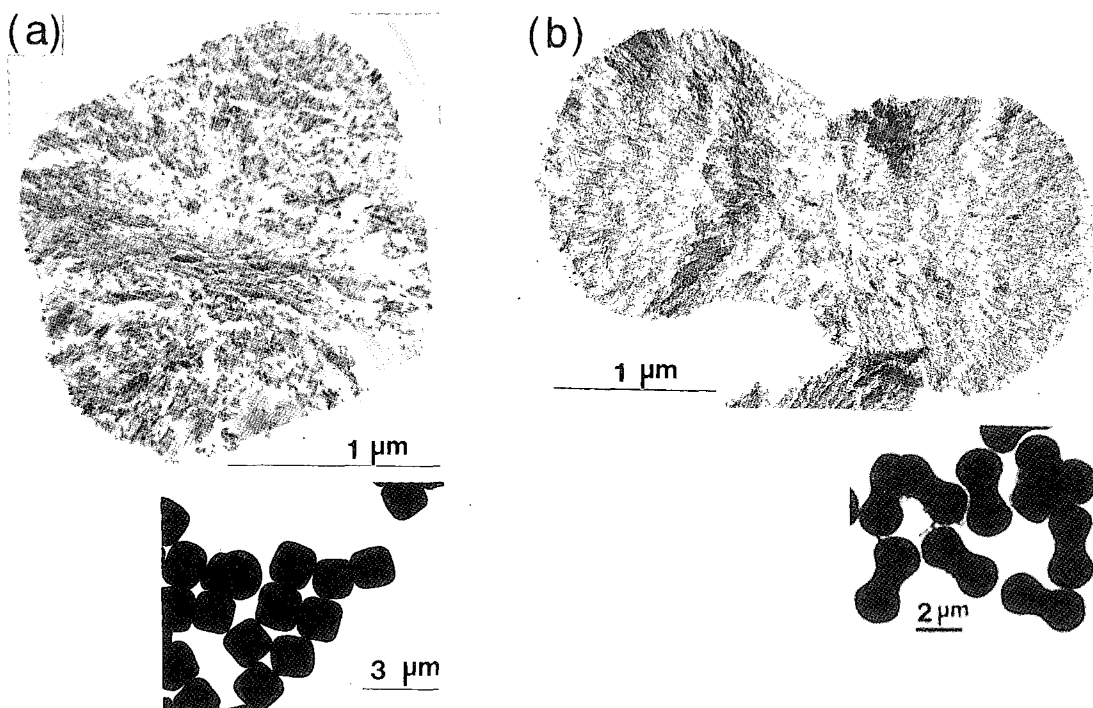

Fig. 5. Transmission electron micrographs of the sections of pseudocubic (a) and peanut-type (b) hematite particles. In each inset, the original particles without slicing are shown, respectively.

particle as schematically indicated in Fig. 4(c).

Fig. 5(a) and (b) show electron micrographs of sections of pseudocubic and peanut-type particles together with the groups of the original particles in below. In the micrograph of the thin section of the pseudocubic particle in Fig. 5(a), there are small subcrystals 10 to 20 nm in size lining up outwards from the center of the particle. In the micrograph of the thin section of the peanut-type particle in Fig. 5(b), the subcrystals are elongated and radially oriented from the rotational axis of the particle. To gain insight into more detailed arrangements and crystallographic orientations of subcrystals of pseudocubic and peanut-type particles, HREM study has been carried out with a high-voltage electron microscope and the HREM images of these two particles are presented in Fig. 6(a) and (b), respectively. The images clearly show the shapes of the subcrystals in pseudocubic and peanut-type particles on atomic scale being completely different from each other. Thus it can be found that the preparation of successive thin sections with an ultramicrotome and their observation by HREM are very useful to make clear three dimensional atomic arrangement of these fine oxide particles and their growth mechanism which can not be analyzed so far.

Quantitative Analysis in Electron Microscopy

1. Computer system for image analysis

In order to easily handle a huge amount of the image data obtained with the new recording system, the efficient computer network system is indispensable. Fig. 7 shows the constitution of

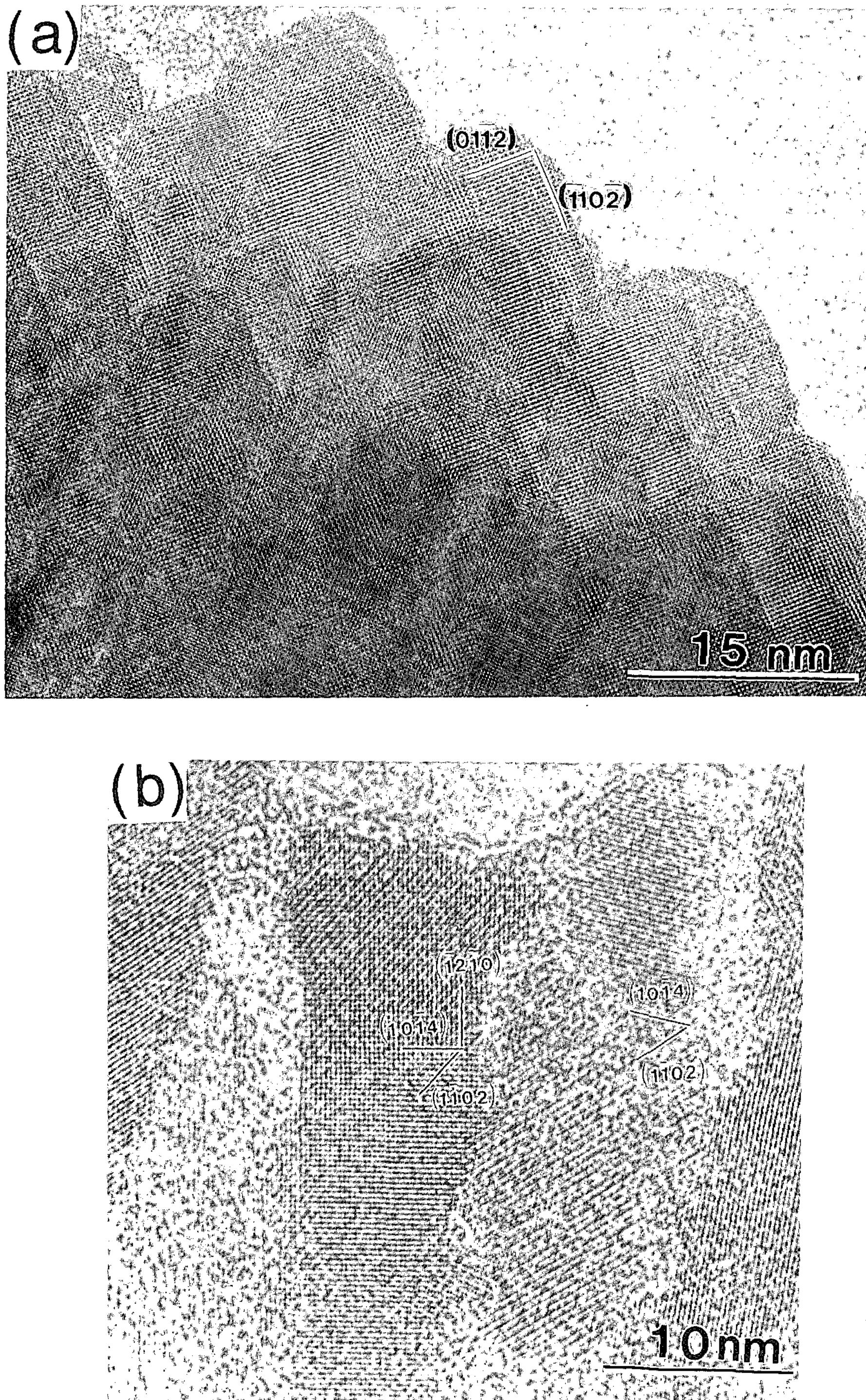

Fig. 6. High-voltage, high-resolution electron microscope images of the parts of the sections of pseudocubic (a) and peanut-type (b) hematite particles.

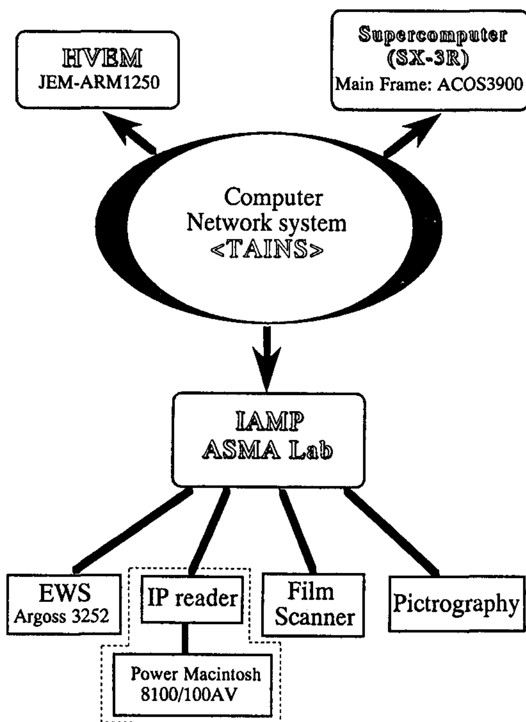

Fig. 7. Constitution of the computer system for image analysis.

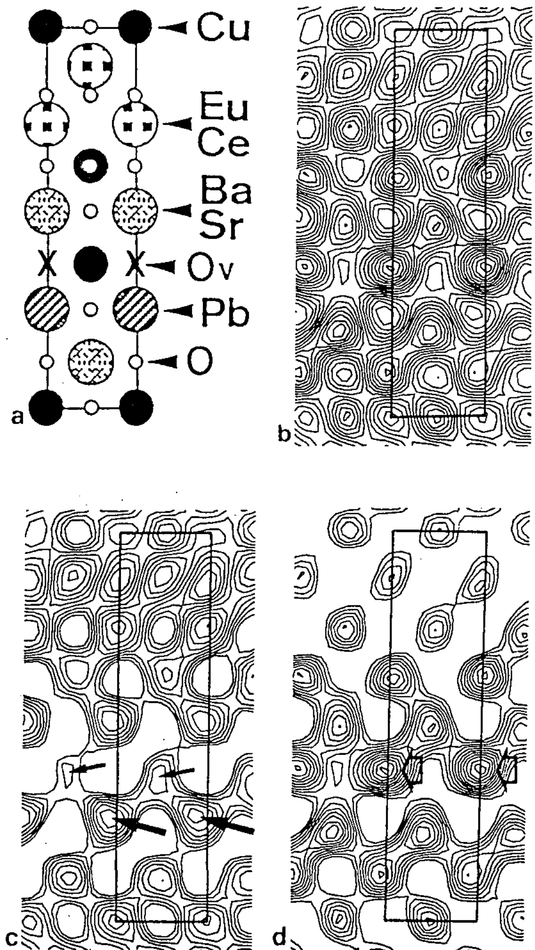

Fig. 8. (a) Structure model of $Pb(Ba,Sr)_2(Eu,Ce)_2Cu_3O_y$.
(b) The intensity distribution of the HREM image with a contour map.
(c) Lower intensity distribution of the image.
(d) Higher intensity distribution of the image.
Crosses in (a) indicate the vacant oxygen position (Ov). Large and small dark arrows in (c) correspond to Pb and Cu atomic columns, respectively. Large open arrows in (d) indicate the vacant oxygen positions.

the computer system for image analysis. Based on UNIX operating system, the computer terminal (Argoss 3252) in the atomic scale morphology analysis (ASMA) laboratory is connected through the network system (TAINS) with the high-voltage electron microscope (HVEM) and a main frame (ACOS 3900) including a supercomputer (SX-3R) at the computer center, Tohoku university, respectively. By using the main frame, we are easily handle a huge amount of imaging plate (IP) data, i.e., 3760×3000 pixels, 16384 gray level, and analyze the data with the software already developed in the main frame (Shindo *et al.*, 1995). By using this system, we can process and store the digital data obtained with the imaging plate as well as the conventional EM films. The system can be also used for the quantitative analysis of the imaging plate data of high-resolution electron microscope images and electron diffraction patterns obtained by conventional electron microscopes as will be shown in the following sections.

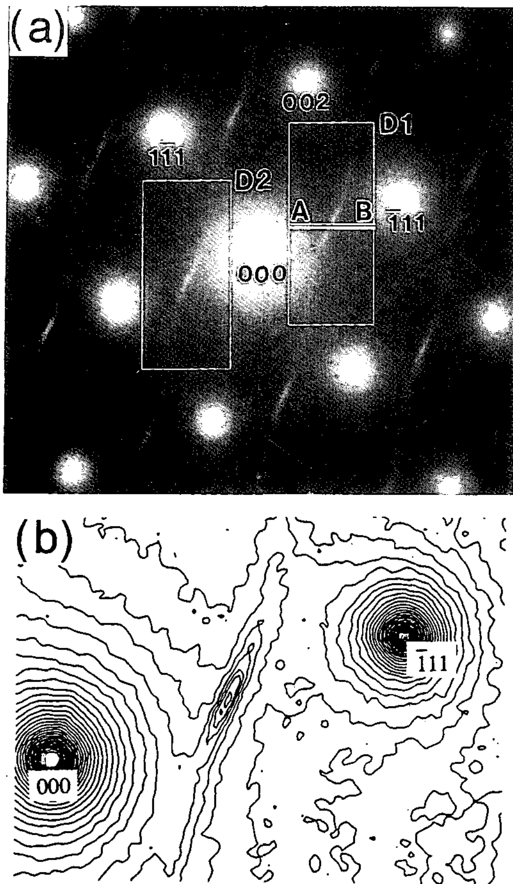

Fig. 9. (a) Electron diffraction pattern of $Ga_{0.5}In_{0.5}P$, observed with the imaging plate.
(b) A part of the electron diffraction pattern (a) shown with a contour map.

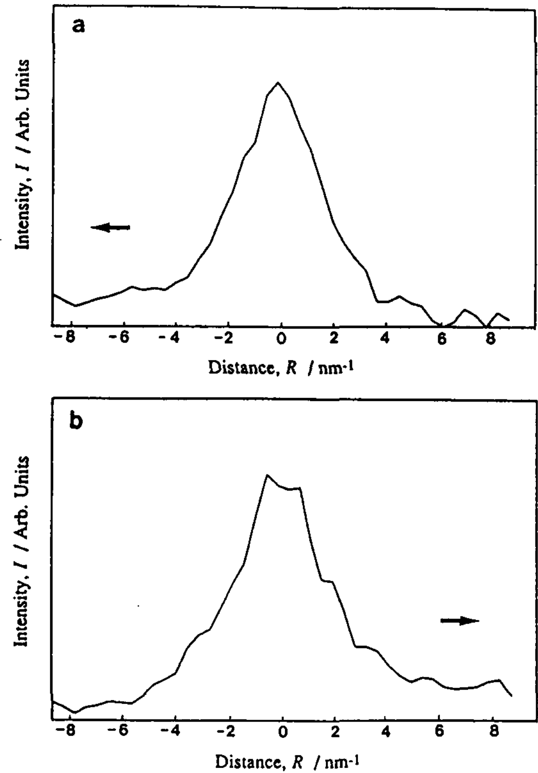

Fig. 10. (a) Ridge of the diffuse scattering peak projected along the horizontal line in D1 of Fig. 9 (a).
(b) Ridge of the diffuse scattering peak projected along the horizontal line in D2 of Fig. 9 (a).

2. Quantitative analysis of high-resolution image

One of the most interesting applications of the quantitative analysis of HREM images with the imaging plate is the structure analysis of layered Cu oxides, which are related to the high-T_c superconductors (Shindo *et al.*, 1991, 1994). An example of HREM images of $Pb(Ba,Sr)_2(Eu,Ce)_2Cu_3O_y$ observed with the imaging plate is shown in Fig. 8(b)-(d) comparing with a structure model proposed by X-ray diffraction study of Fig. 8(a). A contour map of Fig. 8(b) shows whole intensity of the HREM image. In order to examine the intensity distribution more easily, we separated the contour maps into two parts by using the present image processing system. Low and high intensity regions of Fig. 8(b) are shown in Fig. 8(c) and (d), separately. Dense contour lines in Fig. 8(c) indicate the atomic columns of heavy elements, whereas dense contour lines in Fig. 8(d) indicate the lower potential regions. According to these results, we can distinguish Pb atomic columns from Cu atomic columns and locate the vacant oxygen positions between the Cu atomic columns in a wide area of the HREM image.

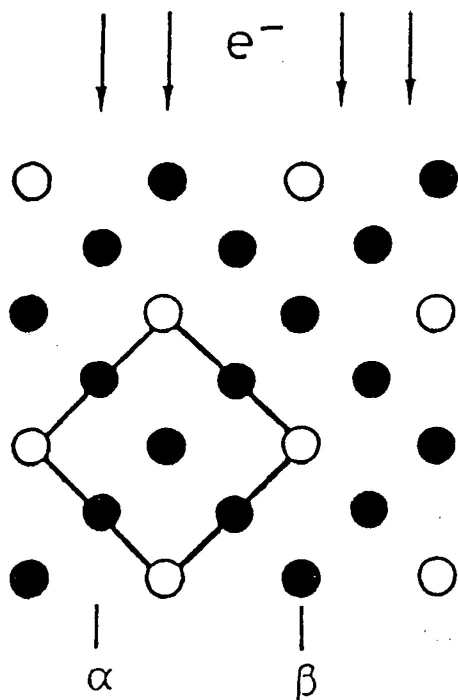

Fig. 11. Atomic arrangement of $Ni_{75}Al_{25}$ with the $L1_2$-type ordered structure projected along the [001] direction, showing alternate ($\bar{1}10$) planes (α and β) parallel to the electron beam.

3. Quantitative analysis of electron diffraction pattern

In the quantitative analysis of electron diffraction patterns, it is very interesting to investigate intensity of superlattice reflections and short-range order diffuse scattering to get structural information of ordering or disordering process (Shindo *et al.*, 1990, 1993). It has been noted that the dynamical diffraction effect is relatively small on the weak scattering and thus the change of intensity of these superlattice reflections and diffuse scattering may be directly connected to the ordered state as discussed in detail previously (Shindo *et al.*, 1982, 1988).

Fig. 9(a) shows an electron diffraction pattern of $Ga_{0.5}In_{0.5}P$ by the IP with the incident electron beam parallel to the [110] direction. There are wavy diffuse scatterings between strong fundamental reflections, as clearly observed in the square regions D1 and D2. Fig. 9(b) shows a contour map of a part of the electron diffraction pattern of (a). The diffuse scatterings have fairly strong intensity on slightly curved lines,

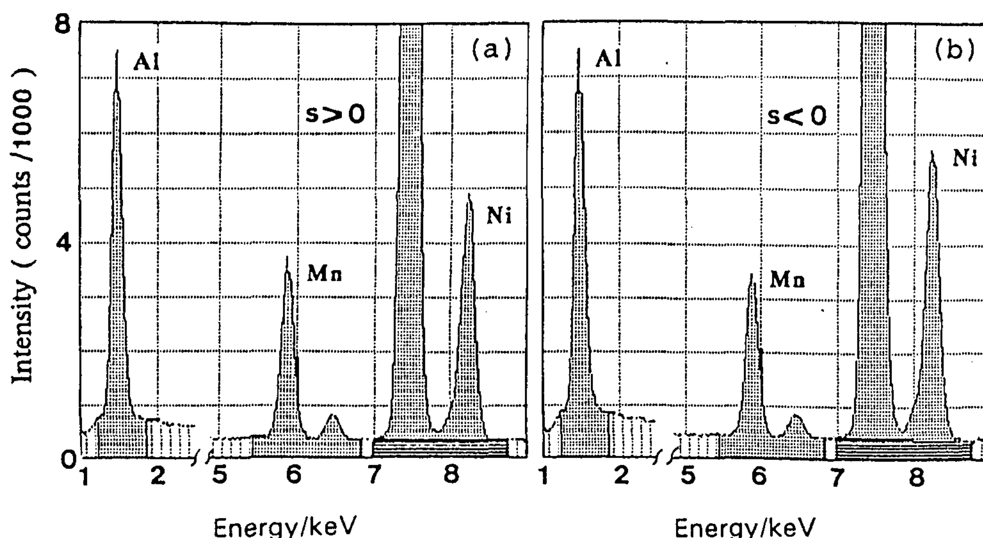

Fig. 12. Characteristic X-ray spectra of the annealed $Ni_{75}Al_{20}Mn_5$ on two diffraction conditions, (a) $s>0$, and (b) $s<0$.

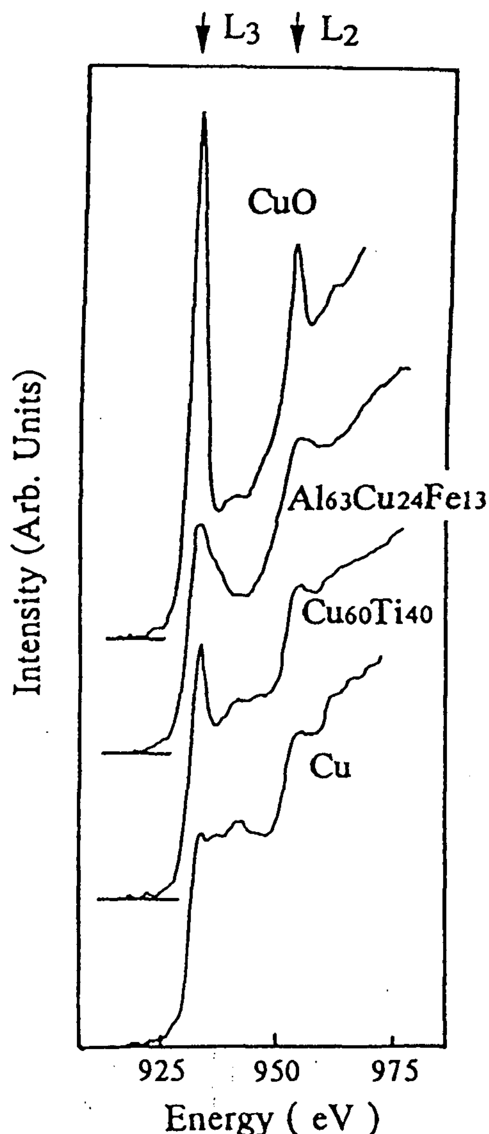

Fig. 13. Energy loss spectra of Cu, $Cu_{60}Ti_{40}$, $Al_{63}Cu_{24}Fe_{13}$ and CuO.

and have intensity maxima around the reciprocal lattice points, such as (−1/2, 1/2, 1/2). It was reported that the intensity distribution of the diffuse scattering changes under different growth conditions. As clearly indicated in Fig. 9(b), there exists a fairly strong background around the transmitted beam in the electron diffraction pattern. The background is consi-dered to be contributed by the thermal diffuse scattering and the scattering due to the plasmon excitation.

In order to analyze the detailed intensity distribution of the diffuse scattering and to get the Warren-Cowley short-range-order parameters from it, the background intensity has to be subtracted. Fig. 10(a) and (b) show the ridge of the diffuse scattering peak projected along the horizontal line A-B in D1 and D2 of Fig. 9(a) after subtracting the background. The zero points of distance as seen in Fig. 10(a) and (b) are corresponding to the reciprocal lattice points of (−1/2, 1/2, 1/2) and (1/2, −1/2, −1/2), respectively. Besides, the arrows indicate the directions of the high scattering angle. It is seen that the peaks of the diffuse scattering are clearly shifted from the zero points and the intensity maxima of the diffuse scattering are the high scattering angle side. The characteristic features of the shape and the intensity distribution of the diffuse scattering can be attributed to the atomic displacement as well as the arrangement of the small ordered domains. It is considered that the atomic displacement results from the different length of bond between Ga-P and In-P. Thus, it is demonstrated that the quantitative analysis of electron diffraction patterns is effective in clarifying not only the superlattice structures but also the short-range-ordered structures of advanced materials such as III-V semiconductors.

Analytical Electron Microscopy

1. ALCHEMI

The energy dispersive X-ray spectroscopy (EDXS) of analytical electron microscopy has been widely used for the compositional analysis of various compounds. Recently, Spence and

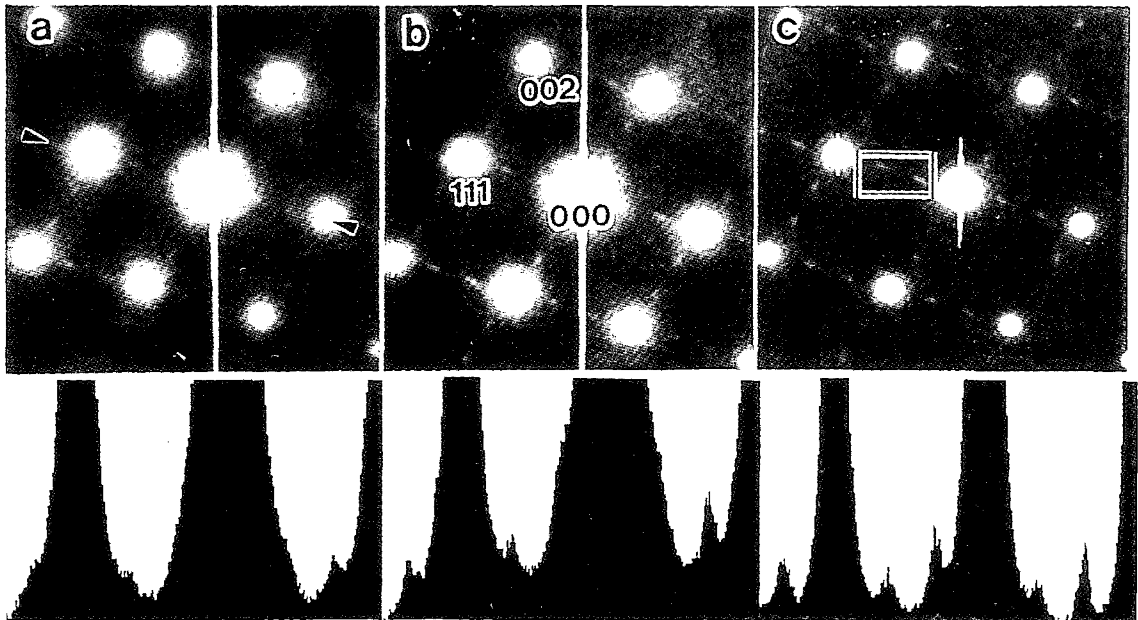

Fig. 14. Electron diffraction patterns of $Al_{0.5}In_{0.5}As$ observed (a) at room temperature without energy filtering, (b) at 107 K without energy filtering and (c) at 107 K with energy filtering by selecting the scattered electrons with the energy loss $-5\,eV<E<5\,eV$. Streaks appearing around the transmitted beam are the artifact due to the intensity saturation in the slow scan CCD camera.
At the bottom of each diffraction pattern, intensity profile at the region between two arrows of (a) is presented.

Taft*Φ* (Spence and Taft*Φ*, 1983) have demonstrated that the crystallographic site of minor element contained in a compound can be determined by a new technique named ALCHEMI (Atom Location by CHannelling Enhanced MIcroanalysis). This method is based on the electron channelling effect that the incident electron beam has different intensities according to the kind of atomic planes. Here, we review ALCHEMI on Ni-Al-Mn (Shindo *et al*., 1990).

The atomic arrangement of $Ni_{75}Al_{25}$ having the L12 type structure, projected along the [001] direction, is shown in Fig. 11, where Ni and Al atoms are indicated by full and open circles, respectively. The incident electron beam is set to be nearly parallel to the $(\bar{1}10)$ planes, which consist of two types of planes, i.e, α-plane composed of only Ni atoms and β-plane composed of both Ni and Al atoms.

EDXS spectra of the annealed $Ni_{75}Al_{20}Mn_5$ on two diffraction conditions (deviation parameter, $s>0$, $s<0$) are shown in Fig. 12, where the peak intensity of Al in both spectra is set to be equal. Comparing the two spectra, the X-ray intensity of Ni on the second diffraction condition ($s<0$) is much higher than that of the first one ($s>0$). The difference directly shows the electron channelling effect on planar channelling conditions. It is noted that the X-ray intensity of Mn does not change so much as that of Ni from one to the other. In order to evaluate the occupation fraction quantitatively, we obtained X-ray intensities on a non-channelling condition where no low order reflections were strongly excited. With these X-ray spectra, we evaluated the site occupancy, k, of Mn atoms at the

Ni site as shown in the previous paper (Shindo *et al.*, 1988).

The results show that the occupation fractions of Mn atoms at the Ni sites are 2% (statistical error: ±14%) in the annealed $Ni_{75}Al_{20}Mn_5$, 25% (statistical error: ±18%) in the quenched $Ni_{75}Al_{20}Mn_5$ and 26% (statistical error: ±23%) in the annealed $Ni_{75}Al_{16}Mn_9$. These results indicate the disordering ratio, i.e., a ratio of the host element Ni occupying the Al site, increases with the increase of the Mn concentration or by quenching the compound.

2. Electron energy loss spectroscopy

Electron energy loss spectroscopy (EELS) is usually used to identify constituent elements and/ or composition of compounds similar to EDXS. However, EELS has the higher energy resolution, i.e, about 1 eV (capital) compared to about 150 eV of EDXS. By using this high energy resolution of EELS, low-loss spectroscopy (zero loss peak and plasmon peak) can be applied to measure sample thickness with high accuracy while core level spectroscopy has been successfuly applied to investigate the electronic structure, especially the unoccupied density of states near the Fermi level. Here, the results of the EELS study of Cu $L_{2,3}$ near-edge fine structures of Cu compounds are presented (Shindo *et al.*, 1993). The EELS study was carried out with a JEM-200CX electron microscope with an accelerating voltage of 200 kV. Energy loss electrons were detected in an image mode with a highly efficient parallel detector (Gatan 666). The full width at half the maximum (FWHM) of the zero loss beam is about 1.8 eV.

Fig. 13 shows the energy loss spectra of one of the typical amorphous materials, $Cu_{60}Ti_{40}$ and that of quasicrystals, $Al_{63}Cu_{24}Fe_{13}$. $L_{2,3}$ edges of Cu and CuO are also shown in Fig. 13 for comparison and the positions of L3 and L2 edges are indicated by arrows at the top of the figure. Since Cu has the fully occupied 3d band, there are no sharp peaks showing a distinct difference with that of CuO where large white lines are observed due to the partially occupied 3d band ($3d^9$). $L_{2,3}$ edges of $Cu_{60}Ti_{40}$ and $Al_{63}Cu_{24}Fe_{13}$ are between those two typical ones in likeness, and they have rather small white lines. It is considered that the white lines of $Cu_{60}Ti_{40}$ mainly result from the charge transfer between Cu-3d and Ti-3d bands as is the case of in $Cu_{60}Zr_{40}$ (Peason *et al.*, 1988). In the case of $Al_{63}Cu_{24}Fe_{13}$, it is also considered that there is some charge transfer between 3d bands of Cu and Fe. However, there is a distinct difference in the $L_{2,3}$ edges of $Al_{63}Cu_{24}Fe_{13}$ from that of $Cu_{60}Ti_{40}$, i.e., FWHM of L3 lines of $Al_{63}Cu_{24}Fe_{13}$ is much wider than those of CuO and $Cu_{60}Ti_{40}$. FWHM of CuO, $Cu_{60}Ti_{40}$ and $Al_{63}Cu_{24}Fe_{13}$ are about 3.1 eV, 2.3 eV and 4.0 eV, respectively. Since FWHM of the zero loss is about 1.8 eV, the above values of FWHM can not be directly correlated with the band width of the unoccupied density of state. Nevertheless it is said that FWHM of the Cu $L_{2,3}$ edge of $Al_{63}Cu_{24}Fe_{13}$ is much wider than that of $Cu_{60}Ti_{40}$. It may be reasonable that the above difference of Cu $L_{2,3}$ edge between $Cu_{60}Ti_{40}$ and $Al_{63}Cu_{24}Fe_{13}$ results from the existence of Al.

3. Energy filtering

Recently, the energy filter systems can be installed in electron microscopes with the development of various types of electron energy loss spectrometers (Gubbens *et al.*, 1994; Uhlemann *et al.*, 1994). The images of TEM were usually contributed by inelastically scattered electrons as well as elastically scattered electrons. Removing all inelastically scattered

electrons from the image with a filter can give rise to better contrast and resolution due to the reduction of background by plasmon and phonon scattering events. Thus electron diffraction patterns with low background may be obtained by selecting the elastically scattered electrons with the energy filter. It was reported that ordered structures appeared in III-V compounds and the anomaly of the band gap energy was closely connected to the ordered structures which were characterized by diffuse scattering as well as by superlattice reflections (Gomyo *et al.*, 1988). In this study, electron diffraction patterns of III-V compounds showing diffuse scattering due to short-range ordering were observed using the energy filter (Zeiss-EM912-Omega) and cold stage. Energy filtered electron diffraction patterns were recorded by the slow scan CCD camera and the imaging plates.

Fig. 14(a)-(c) show electron diffraction patterns of $Al_{0.5}In_{0.5}As$ observed under different conditions. Diffraction patterns of Fig. 14(a) and (b) were observed at room temperature and at 107 K without energy filtering. On the other hand, the diffraction pattern of Fig. 14(c) was observed at 107 K with the energy filter, selecting the scattered electrons with the energy loss -5 eV$<$E$<$5 eV. Intensity profiles in the region between the arrows in the diffraction pattern of Fig. 14(a) are presented at the bottom of each diffraction pattern. By comparing these three diffraction patterns, it is clearly seen that the diffraction pattern of Fig. 14(c) is the most sharp with low background and the detailed intensity distribution of diffuse scattering is well observed. It is concluded from these results that the background around the transmitted beam is reduced effectively by reducing the plasmon scattering rather than the thermal diffuse scattering (Shindo *et al.*, 1995). Thus, it is demonstrated that the electron diffraction study with energy filtering is quite effective in clarifying ordered structures of III-V semiconductors.

Concluding Remarks

Recent transmission electron microscopy in materials analysis was outlined based mainly on the experimental results of ASMA (atomic scale morphology analysis) laboratory in Institute for Advanced Materials Processing, Tohoku university. It is noted that the transmission electron microscopy has achieved rapid progress not only the electron microscopes themselves but also the peripheral instruments. Moreover, new techniques in analytical electron microscopy are reviewed together with rapid developments in specimen preparation techniques.

Acknowledgments

The authors wish to thank Professor Yoshio Waseda, Institute for Advanced Materials Processing, Tohoku University. One of the authors (G.S. Park) gratefully acknowledges the financial support through the Monbusho Scholarship of the Ministry of Education, Science and Culture, Japan.

REFERENCES

Bando Y, 1994. Subnanometer level analysis by 300 kV FE-ATEM. Proc. 13th Int Cong. on Electron Microscopy, Les Editions de Physique Les Ulis, Paris, vol. 1, pp. 591-594.

Fan GY, Ellisman MH, 1993. High-sensitivity lens-coupled slow-scan CCD camera for transmission electron microscopy. Ultramicroscopy. 52, 21-29.

Gomyo A, Suzuki T, Iijima S, 1988. Observation of strong ordering in $Ga_xIn_{1-x}P$ alloy semiconductors. Phys. Rev. Letter. 60, 2645-2648.

Gubbens AJ, Krivanek OL, 1994. Design and performance of a high voltage imagingfilter. Proc. 13th Int. Cong. on Electron Microscopy., Les Editions de Physique Les Ulis, Paris, vol. 1, pp.165-166.

Ishizuka K, 1993. Analysis of electron image detection efficiency of slow-scan CCD cameras. Ultramicroscopy. 52, 7-20.

McMahon G, Malis T, 1993. TEM specimen preparation of nanophase materials by ultramicrotomy. Proc. Electron Microscopy and Analysis, England, pp.349-352.

Mori M, Oikawa T, Miyahara J, Harada Y, 1990. Development of the imaging plate for the transmission electron microscope and its characteristics. J. Electron Microscopy. 39, 433-436.

Oikawa T, Mori N, Takano N, Harada Y, Ohnishi M, 1990. The development of an image-recording system using the imaging plate in a TEM. J. Electron Microscopy. 39, 437-443.

Otten MT, 1994. Performance of the CM200 FEG. Proc. 13th Int. Cong. on Electron Microscopy, Les Editions de Physique Les Ulis, Paris, vol. 1, pp.235-236.

Pantel R, Auvert G, Mascarin G, Gonchond JP, 1994. Advanced CMOS silicon technology analysis using focused ion beam etching and transmission electron microscopy observation. Proc. 13th Int. Cong. on Electron Microscopy, Les Editions de Physique Les Ulis, Paris, vol. 1, pp.1007-1008.

Park GS, Shindo D, Waseda Y, Aoyagi E, Aita S, 1994. High-voltage, high-resolution electron microscopy on thin sections of fine oxide particles. Proc. 13th Int. Cong. on Electron Microscopy, Les Editions de Physique Les Ulis, Paris, pp.805-806.

Park GS, Shindo D, Waseda Y, Sugimoto T, 1996. Internal structure analysis of monodispersed pseudocubic hematite particles by electron microscopy. J. Colloid InterfaceSci. 177, 198-207.

Park GS, Shindo D, Waseda Y, 1994. High-voltage, high-resolution electron microscopy on thin sections of monodispersed pseudocubic hematite particles. J. Electron Microscopy 43, 208-212.

Park GS, Shindo D, Waseda Y, Yang JM, Oikawa T, Kersker M, 1995. Preparation of successive thin sections of fine oxide particles by an ultramicrotome. Proc. 53rd Annual MSA /HCS Meeting, Kansas City, pp.508-509.

Park GS, Shindo D, 1996. Evaluation of a spherical aberration constant of the objective lens of HVEM at Tohoku University. J. Electron Microscopy 45, 152-158.

Peason DH, Fults B, Ahn CC, 1988. Measurements of 3d state occupancy in transition metals using electron energy loss spectroscopy. Appl. Phys. Letter. 53, 1405-1407.

Petres JJ, Dezelic G, Tezak B, 1969. Monodisperse sols of barium sulfate. III. Electron-microscopic study of internal structure of particles. Croatica Chemica Acta. 41, 183-186.

Saka H, Kuroda K, Hong MH, Kamino T, Yaguchi T, Tsuboi H, Ishitami T, Koike H, Shibuya A, Adachi A, 1994. Fabrication of cross sectional TEM specimens of metallic materials using a focused ion beam. HREM of interfaces in a hot dip galvanized steel. Proc. 13th Int. Cong. on Electron Microscopy, Les Editions de Physique Les Ulis, Paris, vol. 1, pp.1009-1010.

Shindo D, Lee BT, Waseda Y, Muramatsu A, Sugimoto T, 1993. Crystallography of platelet-type hematite particles by electron microscopy. Materials Transactions 34, 580-585.

Shindo D, Park GS, Waseda Y, Sugimoto T, 1994. Internal structure analysis of monodispersed peanut-type hematite particles produced by the gel-sol method. J. Colloid Interface Science 168, 478-484.

Shindo D, Park GS, 1995. Structure analysis of fine oxide particles by high-voltage, high-resolution electron microscopy. Proc. 2nd Pacific Rim Int. Conf. on Advanced Materials and Processing, Korea, pp.1089-1092.

Shindo D, Oku T, Kudoh J, Oikawa T, 1994.

Quantitative high-resolution electron microscopy of a high-T_c superconductor $Tl_2Ba_2Cu_1O_y$ with the imaging plate. Ultramicroscopy 54, 221-228.

Shindo D, Hiraga K, Oku T, 1991. Quantification in high-resolution electron microscopy with the imaging plate. Ultramicroscopy 39, 50-57.

Shindo D, Hiraga K, Oikawa T, Mori N, 1990. Quantification of electron diffraction with imaging plate. J. Electron Microscopy 39, 449-453.

Shindo D, Kudoh J, Iijima S, Oikawa T, Nemoto Y, 1993. High-resolution electron microscopy of short-range ordered structure of $Ga_{0.5}In_{0.5}P$. J. Japan Inst. Metals. 57, 1385-1389.

Shindo D, 1982. High-resolution images of ordered alloys by high-voltage electron microscopy. Acta Crystallography A38, 310-317.

Shindo D, Hirabayashi M, 1988. Dynamical diffraction effects on high-resolution electron microscopy of ordered alloys. Acta Crystallography A44, 954-960.

Shindo D, Hiraga H, Takasugi T, Tsai AP, 1990. Electron channelling enhanced microanalysis on Ni-Al-Mn and Al-Mn-Si. Materials Transactions, JIM 31, 647-651.

Shindo D, Kikuchi M, Hirabayashi M, Hanada S, Izumi O. 1988. Site determination of Fe. Co and Cr atoms added in Ni_3Al by electron channelling enhanced microanalysis. Trans. Japan Inst. Metals. 29, 956-961.

Shindo D, Hiraga K, Tsai AP, Chiba A, 1993. Cu $L_{2,3}$ white lines of Cu compounds studied by electron energy loss spectroscopy. J. Electron Microscopy 42, 48-50.

Shindo D, Spence JCH, Gomyo A, 1995. Evaluation of electron diffuse scattering by energy filtering. Proc. 2nd Pacific Rim Int. Conf. on Advanced Materials and Processing, Korea, pp. 1077-1080.

Spence JCH, TaftΦ J, 1983. ALCHEMI : a new technique for locating atoms in small crystals. J. Microscopy 130, 147-154.

Uhlemann S, Rose H, 1994. Comparison of the performance of existing and proposed imaging energy filters. Proc. 13th Int. Cong. on Electron Microscopy, Les Editions de Physique Les Ulis, Paris, vol. 1, pp. 163-164.

Watson JHL, Cardell RR, Jr., Heller W, 1962. The internal structure of colloidal crystals of β-FeOOH and remarks on their assemblies in schiller layers. J. Phys. Chemistry 66, 1757-1763.